Journal of Microscopy

Journal of Microscopy, Vol. 280, Issue 2 2020, pp. 86–103 doi: 10.1111/jmi.12957
Received 22 May 2020; accepted 23 August 2020

Functional organisation of the endomembrane network in the digestive gland of the Venus flytrap: revisiting an old story with a new microscopy toolbox

C. BOULOGNE*, C. GILLET*, L. HUGHES†,‡, R. LE BARS*, A. CANETTE§, C.R. HAWES† & B. SATIAT-JEUNEMAITRE*

*Université Paris-Saclay, CEA, CNRS, Institute for Integrative Biology of the Cell (I2BC), Gif-sur-Yvette, France
†Oxford Brookes University, Oxford UK, England
‡Oxford Instruments NanoAnalysis, High Wycombe, Bucks, UK
§CNRS, Institut de Biologie Paris-Seine (IBPS), Sorbonne Université, Paris, France

Key words. Array tomography, carnivorous plants, endomembranes, scanning electron microscopy, serial block face, serial sections, tomography, transmission electron microscopy.

Summary

Up-to-date imaging approaches were used to address the spatiotemporal organisation of the endomembrane system in secretory cells of *Dionaea muscipula*. Different 'slice and view' methodologies were performed on resin-embedded samples to finally achieve a 3D reconstruction of the cell architecture, using ultrastructural tomography, array tomography, serial block face-scanning electron microscopy (SBF-SEM), correlation, and volume rendering at the light microscopy level. Observations of cryo-fixed samples by high-pressure freezing revealed changes of the endomembrane system that occur after trap activation and prey digestion. They provide evidence for an original strategy that adapts the secretory machinery to a specific and unique case of stimulated exocytosis in plant cells. A first secretion peak is part of a rapid response to deliver digestive fluids to the cell surface, which delivers the needed stock of digestive materials 'on site'. The second peak of activity could then be associated with the reconstruction of the Golgi apparatus (GA), endoplasmic reticulum (ER) and vacuolar machinery, in order to prepare for a subsequent round of prey capture. Tubular continuum between ER and Golgi stacks observed on ZIO-impregnated tissues may correspond to an efficient transfer mechanism for lipids and/or proteins, especially for use in rapidly resetting the molecular GA machinery. The occurrence of one vacuolar continuum may permit continuous adjustment of cell homeostasy. The subcellular features of the secretory cells of *Dionaea muscipula* outline key innovations in the organisation of plant cell compartmentalisation that are used to cope with specific cell needs such as the full use of the GA as a protein factory, and the ability to create protein reservoirs in the periplasmic space. Shape-derived forces of the pleiomorphic vacuole may act as signals to accompany the sorting and entering flows of the cell.

In Memoriam of Chris Hawes : *Even more impressive than the amount of electron micrographs that Chris published over the years is the number of unpublished micrographs that he kept nicely ordered in his filing cabinet. Among them were preliminary studies describing the endomembrane system of Dioneae muscipula, dating from the time when Chris was working at the Plant Science University in Oxford, in partnership with Barry Juniper in the 1980s. He was very keen to apply the ZIO impregnation protocol to various botanical samples in order to make observations by High Voltage Transmission Electron Microscopy (HVTEM) (Hawes, 1981). Two plates describing the endomembrane system of Dionaea were published at the time* (Juniper *et al.*, 1982). *Many years later, these very same pictures served as the basis for many animated discussions in Chris's office on the complexity of the plant endomembrane system. Thus, when the era of 3D SEM arrived, Chris was very proud to bring out his 35-year-old resin blocks, as the ZIO-induced contrast was perfect for the SBF-SEM approach. This paper proposes to resume the work developed in our two laboratories based on the biology of Dionaea, and to act as a way to acknowledge Chris's enthusiasm for plant wonders, plant endomembrane complexity, and his love for electron microscopy.*

Correspondence to: B. Satiat-Jeunemaitre, Université Paris-Saclay, CEA, CNRS, Institute for Integrative Biology of the Cell (I2BC), 91198 Gif-sur-Yvette, France. Tel: 00 33 1 69 82 46 60; e-mail: bsj@i2bc.paris-saclay.fr

Introduction

The fascination for carnivorous plants has produced many writings, both in fiction and scientific literature. Indeed, the variety in form and physiological behaviour of these plants is remarkable enough to stimulate the imagination, as well as endless observations at the macroscopic and microscopic levels. For the cell biologist, the secretory machinery of carnivorous plants is an amazing experimental model to work on, as this is one of the rare plant examples in which secretion of high levels of proteins may be triggered by prey capture.

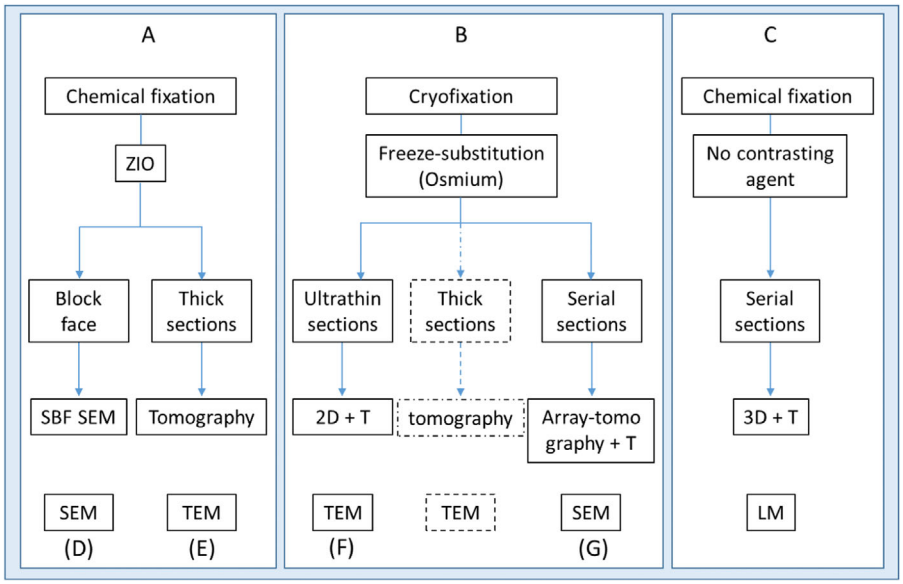

Fig. 1. Flowchart of the microscopy approaches developed to explore Dionaea secretory cell architecture. Boxes (A)–(C) represent distinct embedding protocols. (D), (E), (G) Distinct 'slice and view' approaches for 3D-EM reconstruction (respectively SBF-SEM (D), TEM tomography (E) and array tomography-SEM (G)). (F) 2D + T = 2D study comparing three stages of the digestive cycle over time (T). Broken lines: see complementary protocol for TEM-tomography in Gergely *et al.* (2018).

Research on carnivorous plants has called upon a large tradition of microscopy and biochemical approaches over the last century, as recalled in Barry Juniper's magnificent book, *The Carnivorous Plants* (Juniper *et al.*, 1989). More recently, carnivorous plant research has benefited from the sequencing of various other species (Fukushima *et al.*, 2017). However, correlations between potential molecular machineries, biochemical data, and ultrastructural features are still missing.

How do the secretory cells of carnivorous plants reconcile their 'predator' functions and their plant needs? How do they coordinate the production and secretion of huge amounts of digestive enzymes, along with the secretion of polysaccharides and digestive fluids? Tentative answers to such questions must be supported by solid observations of the cell architecture. Transmission electron microscopy (TEM) studies have always been a driving force in suggesting various (sometimes debatable) scenarios for secretion models in the secretory cells of carnivorous plants (Juniper *et al.*, 1989). In light of today's knowledge, it is possible that those controversial analyses may have their sources in the observations of potential artefacts caused by specific TEM sample preparation (both from fixation and the generation of contrast). More importantly, the lack of spatial information provided by 2D data should also be considered as a missing link in the understanding of cell architecture.

The aim of this paper was to use a combination of up-to-date imaging approaches in order to address the spatiotemporal organisation of the endomembrane system in secretory cells (see the flow chart in Fig. 1). Different 'slice and view' methodologies were performed on resin-embedded samples to finally achieve a 3D reconstruction of the cell architecture, using ultrastructural tomography, array tomography, serial block face-scanning electron microscopy (SBF-SEM), correlation and volume rendering at the light microscopy level.

The biological model that we used to investigate the nature of the secretory cascades in glandular cells is *Dionaea muscipula* Ellis, better known as the Venus flytrap. Its first botanical description was made by the naturalist John Ellis in the early eighteenth century in a letter to his colleague Linnaeus, which described the amazing sensitivity and characteristic traits of these plants. Darwin was however the first to initiate rigorous experiments on the trapping mechanisms and digestion processes, reported in his famous book, *Insectivorous Plants* (Darwin, 1875). The prey capture process developed by *Dionaea muscipula* is based on a snap trap mechanism, and the mechanism and physiology of this spectacular process are still being investigated (Volkov *et al.*, 2009). The trap is composed of two lobes that function as a jaw to capture and digest prey. Marginal spikes extend from the margin of the trap lobes. In the resting stage, the trap is open (Fig. 2A). The inner surface of the trap is visible, covered by at least two types of secretory glands occupying distinct territories (Fig. 2A). The alluring glands at the margin of the trap secrete a mixture of carbohydrates to attract the prey, while pigmented digestive glands cover most of the inner surface of the trap (Juniper *et al.*, 1989). When prey make contact with one lobe, they are detected via the stimulation of three hairs in the centre of each lobe of the trap (Fig. 2A, arrow), provoking a rapid closing movement of the two lobes at the mid-rib. Prey are thus trapped in a cage-like structure that ultimately crushes

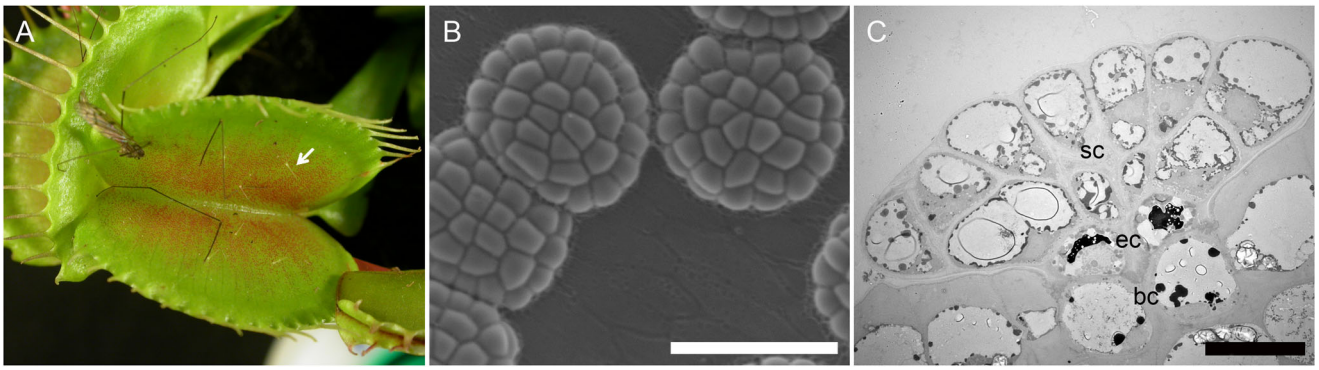

Fig. 2. Main features of the *Dionaea muscipula* snap trap and secretory gland. (A) An open trap of *Dionaea muscipula*. The red pigmented area corresponds to hundreds of digestive glands. Note the hairs (arrow) acting as prey sensors to induce trap closure. (B) SEM micrograph showing the digestive glands in control of enzyme secretion when a prey has been captured. (C) TEM micrograph of a longitudinal section in a digestive gland (sc: secretory cells; ec: endodermoid cells; bc: basal cells). Scale bar in (B): 100 μm; scale bar in (C): 20 μm.

them when the two lobes close in a slow movement (Darwin, 1875). The secretion of enzymes is stimulated by the closure of the trap and the detection of nitrogenous compounds from the prey (Scala *et al.*, 1969; Robins, 1976; Juniper *et al.*, 1989). Prey digestion begins with the delivery of digestive enzymes from the hundreds of digestive glands in contact with the prey. After the immediate capture of the prey, the trap remains closed for 4–5 days before opening again to start a new cycle (Davis *et al.*, 2019). The description of the prey 'digestive cycle' established in the early 1980s (Robins & Juniper, 1980a,1980b,1980c,1980d) remains a solid foundation for today's research. *Dionaea* secretory glands break down particles of nutrients from its prey, providing minerals and nitrogen supplies for the plant's requirements. This process has been related to specific enzymes detected in the *Dionaea* 'digestive fluid' in the 1970s (Scala *et al.*, 1969; Robins, 1976; Lichtner & Williams, 1977). However, the intracellular localisation of the digestive enzymes in gland cells and the events associated with their discharge at the cell surface are still major questions in the field. The fine structure of the secretory cells of *Dionaea* digestive glands was observed by transmission electron microscopy (TEM) during the last decades of the 20th century (Scala *et al.*, 1968; Schwab *et al.*, 1969; Robins & Juniper, 1980a,1980b,1980c,1980d; Juniper *et al.*, 1982). In accordance with the membrane flow concept proposed by Morré (James Morré *et al.*, 1979), it was accepted that secretion is based on exocytotic processes from the endoplasmic reticulum (ER) to the cell surface. Several hypotheses, controversial at the time, have been raised to attribute functional roles to the ER, Golgi apparatus (GA) or vacuoles in carnivorous plant biology (Bal & Payne, 1972; Unzelman & Healey, 1974; Juniper *et al.*, 1989). All of these previous studies were based on chemical fixation, and used various cytochemistry protocols to give contrast to the biological samples.

However, the preference for cryofixation methods over chemical fixation has been emphasised in the last 30 years in order to obtain a better preservation of plant membranes and fewer ultrastructural artefacts in plant cells (Kiss *et al.*, 1990; Samuels *et al.*, 1995; Seguí-Simarro *et al.*, 2004) including *Dionaea muscipula* (Gergely *et al.*, 2018). In addition, the development of methods to reconstruct a volume from 2D images (Hughes *et al.*, 2014; Borrett & Hughes, 2016; Kittelmann *et al.*, 2016) has been essential to revisiting or improving working hypotheses on cell functional organisation and may therefore be a good tool to explore cell architecture of carnivorous plants. Finally, the development of 3D reconstruction by light microscopy approaches based on fluorescent properties (Plachno *et al.*, 2006) may also provide new information regarding the cell organisation.

Here, we used *Dionaea muscipula* as an inducible system to monitor the changes of the endomembrane system that occur after trap activation and prey digestion. Our results provide evidence for an original strategy that adapts the secretory machinery to a specific and unique case of stimulated exocytosis in plant cells.

Material and methods

Plant material and culture conditions

Dionaea muscipula plants were purchased from commercial suppliers. Plants were maintained in green house conditions in a mixture of 2/3 acid peat (pH 4 ± 0.5, see: https://www.puteaux-sa.fr/terreau-potager-tourbe-naturelle-flora-150lt.html) and 1/3 sand (pH 7), and were watered with distilled water.

Induction of secretion

Traps were stimulated with blocks of 2% aqueous gelatin (Sigma G-2500) mimicking the presence of a prey (Schwab

et al., 1969) {Schwab, 1969 #120}.Traps were then removed, dissected in small pieces in the glandular area and fixed for electron microscopy studies just before stimulation (Day 0), and 1, 2, 3 and 5 days after stimulation.

Microscopy

The flow chart presented in Figure 1 summarises the main work flows developed in this study.

Chemical fixation, ZIO impregnation and epoxy resin embedding for TEM and SEM (Fig. 1, Box A). Thin strips of glandular leaves were cut under glutaraldehyde/paraformaldehyde fixative and impregnated by the zinc/iodine/osmium (ZIO) *en bloc* staining protocol as described (Hawes *et al.*, 1981; Juniper *et al.*, 1982). For TEM tomography, 120-nm thick sections were collected on Formvar-coated copper grids.

SBF-SEM (Fig. 1, Box A, column D). The final trimmed blocks were mounted onto 3View stubs (Gatan), and sputter-coated (Agar Scientific sputter coater) with gold for 30 s (thickness layer ~20 nm) in order to improve conductivity. SBF-SEM images were collected on a Merlin Compact scanning electron microscope (Zeiss) with the Gatan 3View system. Section thickness was set to 40–100 nm, depending on the magnification used, and the block face was imaged in variable pressure mode (~50 Pa) at 4 kV acceleration voltage with an aperture size of 30 μm and a pixel dwell time of 2–5 μs. Data processing (stack formation, image alignment, and trimming and scaling of sections to a common mean and SD) was performed using the IMOD software package (Kremer *et al.*, 1996). The Amira software (Thermo) brush tool was used to select the regions of interest around the Golgi and ER, and the VolRen function was applied and thresholded to show maximum intensity 3D views of Golgi bodies and ER (Borrett & Hughes, 2016; Gergely *et al.*, 2018).

Cryofixation by high-pressure freezing and freeze-substitution for TEM and SEM studies (Fig. 1, Box B). Three mm^2 trap fragments were immersed in the cryoprotectant hexadecene. One mm diameter discs were made using a punch and quickly placed in metal dishes (Leica 'flat specimen carriers', 400 μm depth, ref. 16706899). Samples were cryofixed in liquid nitrogen by high-pressure freezing with EMPACT2 (Leica). The cryofixed material was then stored in liquid nitrogen until freeze-substitution.

Freeze-substitution (FS) was performed in the AFS2 apparatus (Leica). Frozen specimens were kept at –90°C in an FS medium of 2% osmium in anhydrous acetone. The temperature was increased as follows: 24 h at –90°C, 15 h from –90°C to –60°C, 8 h at –60°C, 15 h from –60°C to –30°C and 8 h at –30°C. Specimens were then transferred on ice and washed three times in acetone. They were then processed for epoxy resin (LV premix Medium R1165, Agar Scientific, Oxford Instruments) embedding (Hawes & Satiat-Jeunemaitre, 2001; Marion *et al.*, 2017).

Chemical fixation and LR White embedding for light microscopy (Fig. 1, Box C).

Tissue preparation for histology by light microscopy. Leaf pieces were cut and fixed 4–6 h at room temperature with 3% paraformaldehyde and 0.5% glutaraldehyde in 0.1 M cacodylate buffer at pH 6.8. After washing with 0.1 M cacodylate buffer, samples were progressively dehydrated at 4°C in 10%–50% ethanol baths (10%–20%–30%–50%) and then at –20°C in 70%–100% ethanol baths (70%–90%–100%). To achieve complete dehydration, samples were finally kept in absolute ethanol before embedding in acrylic resin (LR White Resin, Agar Scientific, Oxford Instruments) (Hawes & Satiat-Jeunemaitre, 2001).

Sectioning and staining for LM. Embedded trap fragments were cut on an EM UC6 ultramicrotome (Leica Microsystems) with a JUMBO diamond (Diatome), as its large boat facilitates production of section ribbons with no loss or folding. Two hundred and fifty-nanometre sections were directly collected on glass coverslips and stained at RT in DAPI (0.5 mg mL^{-1}) and propidium iodide (PI) (0.5 mg mL^{-1}) solution during 15 min before washing three times with water. After removing excess water, coverslips were mounted on slides with Citifluor AF1 (EMS) and sealed with nail polish. Samples were immediately imaged after staining.

Light microscopy imaging and image analysis. Image acquisitions were performed either on a widefield microscope (DMI6000 B, Leica) equipped with a CCD camera (CoolSNAP HQ2, Photometrics) or on a confocal microscope (SP8-X, Leica) equipped with hybrid detectors. First, a map of the ribbon was established using a 10× objective (Plan Apo, NA: 0.4, Leica) to identify and mark the glands on every leaf section. Then, using a 63× oil immersion objective (Plan Apo, NA: 1.4, Leica), *z*-stacks (*z* step: 300 nm) were automatically created for each gland section. Each stack was acquired sequentially on two channels to collect the fluorescence of both propidium iodide (excitation: 555 nm, detection: 565–700 nm) and DAPI (excitation: 405 nm, detection: 450–500 nm). Each stack was then processed with automated scripts in ImageJ (Schneider *et al.*, 2012). Briefly, stacks were first projected as a maximal intensity projection, and all resulting projections were concatenated to produce one 3D stack for each gland. Then the stacks were realigned using the StackReg plugin (Thevenaz *et al.*, 1998) and corrected for plane-to-plane intensity variations. To perform the segmentation of cell walls and vacuoles, the Ilastik machine learning software was used (Berg *et al.*, 2019) to produce binary masks. To avoid

any segmentation error on the cell wall masks (which can lead to unwanted fusing events), quality control and manual correction steps were essential. Finally, in order to attribute each vacuole to a cell and generate volume rendering, we imported the masks into Imaris (Bitplane). All data presented were extracted cell by cell and analysed in Prism (GraphPad).

TEM (Fig. 1, Box B, column F). Ultrathin (80 nm) or thick (150 nm) sections were cut with an EM UC6 ultramicrotome (Leica Microsystems) and collected on Formvar carbon-coated copper grids. Ultrathin sections were stained with 2% uranyl acetate (Merck) and Reynolds lead citrate (Agar) according to standard procedures (Hawes & Satiat-Jeunemaitre, 2001). Grids were examined under a JEOL 1400 TEM operating at 120 kV (JEOL, http://www.jeol.com). Images were acquired using a high-resolution (11 megapixels), high-speed camera (SC1000 Orius; Gatan, http://www.gatan.com) and processed using Digital Micrograph (Gatan).

Array tomography-SEM (Fig. 1, Box B, column G). To analyse each of the three steps in the digestive cycle, 50–60 nm thick serial sections were cut with a 35° diamond (Diatome) on an EM UC6 ultramicrotome (Leica Microsystems), and deposited on several rectangular 5 × 7 mm silicon wafers (one per ribbon, G3391, Agar Scientific), which were then glued on an aluminium pin stub (Zeiss aluminium short pin stub 25.4 mm diameter top, https://www.microtonano.com) with silver cement. Samples that were previously plasma-cleaned with an Evactron (XEI scientific) were then observed with a Field Emission Scanning Electron Microscope (GeminiSEM 500, Zeiss) driven by SmartSEM, operating in high vacuum at 1.5 kV with the high current mode and a 30 µm aperture diameter, and approximately 1.75 mm working distance. Two detectors (one in-lens and one in-column, respectively) were used to separately collect secondary (SE) and backscattered electrons (energy selective BSE detector with filtering grid between 400 and 750 V). Brightness and contrast LUT (LookUp Table) mode was inverted to obtain TEM-like images.

Automated acquisitions were performed using Atlas 5 (Fibics), with a pixel dwell time of 6.4 µs, a line average of 50, a 7-nm pixel size and 8192 × 8192 pixels image definition (corresponding to an image size of 57.3 × 57.3 µm), overlap at 10% (each ROI was a mosaic of 2 images), autofocus and autoastigmatism. After stitching, stacks were recorded with a 50–50 mix of SE and BSE channels. In these conditions, SE images were generated at the extreme surface (depth of a few nanometres), whereas the BSE images were capable of providing information from a depth of a few tens of nanometres. Images produced by the SE in Lens detector were low-contrasted with good resolution. The SE in Lens is also charge sensitive and detects topological informations like folds, dirts and scan mark (especially in the overlapped regions for mozaïc). On the other hand, images produced by the ESB detector had a better contrast, but a higher background noise. The 50–50 mix of the two channels is a right equilibrium to take advantages of the two detection modes and practically erase their defaults. Prealignment in Z was performed using the 'linear stack alignment with SIFT' module of the 'registration' plugin in Fiji. 3D reconstructions were made using IMOD (Kremer *et al.*, 1996).

Results

The main traits of the Dionaea muscipula *digestive glands, and a chronological map of secretion*

Figure 2 presents the main characteristics of the snap trap mechanism developed by *Dionaea* (cf Introduction paragraph). Our study focuses on the pigmented digestive glands covering most of the inner surface of the trap. Those digestive glands that we investigated are arranged in a highly organised multicellular complex (Fig. 2B). Longitudinal sections observed by conventional TEM (Fig. 2C) highlight this tissue organisation. In accordance with the typical organisation of plant secretory glands (Luttge, 1971), three cell types may be observed: basal cells, which are inserted in the epidermis; endodermoid cells; and secretory cells involved in the synthesis and release of digestive fluid (see also fig. 1B in Gergely *et al.*, 2018).

Our experimental conditions using a gelatine block to simulate the prey present the same kinetics as described by previous authors: after prey capture, the trap rapidly closes and reopens after 4–5 days. We were therefore confident that sampling the traps at day 0 (resting stage before stimulation by contact with the gelatine block), day 1, day 2, day 3 and day 5 would give different snapshots of the secretory system in action, in agreement with the digestive cycle described by Juniper (Juniper *et al.*, 1989).

3D reconstruction of subcellular architecture by TEM tomography and SBF-SEM

A first set of 3D data was acquired from specimens fixed by chemical fixation combined with ZIO impregnation that had already been used in earlier studies (Juniper *et al.*, 1982) (see flow box A in Fig. 1). Strong labelling of the ER and GA was previously described by TEM and stereomicroscopy at 80, 180 and 1000 kV by Chris Hawes (see figs. 18–22 in Juniper *et al.*, 1982). It is widely accepted that the ZIO reaction may impregnate membranes in highly differential ways across a sample (probably due to an uneven penetration of the ZIO mixture which may be associated with a former uneven chemical fixation speed across the samples or the cells). In the former study, observations were performed on Golgi stacks that had been evenly stained across the cisternal stack, whereas our TEM tomography study concentrated on Golgi stacks exhibiting a gradual staining from *cis* to *trans* cisternae. The transverse sections of Golgi stacks (Fig. 3B) clearly show a

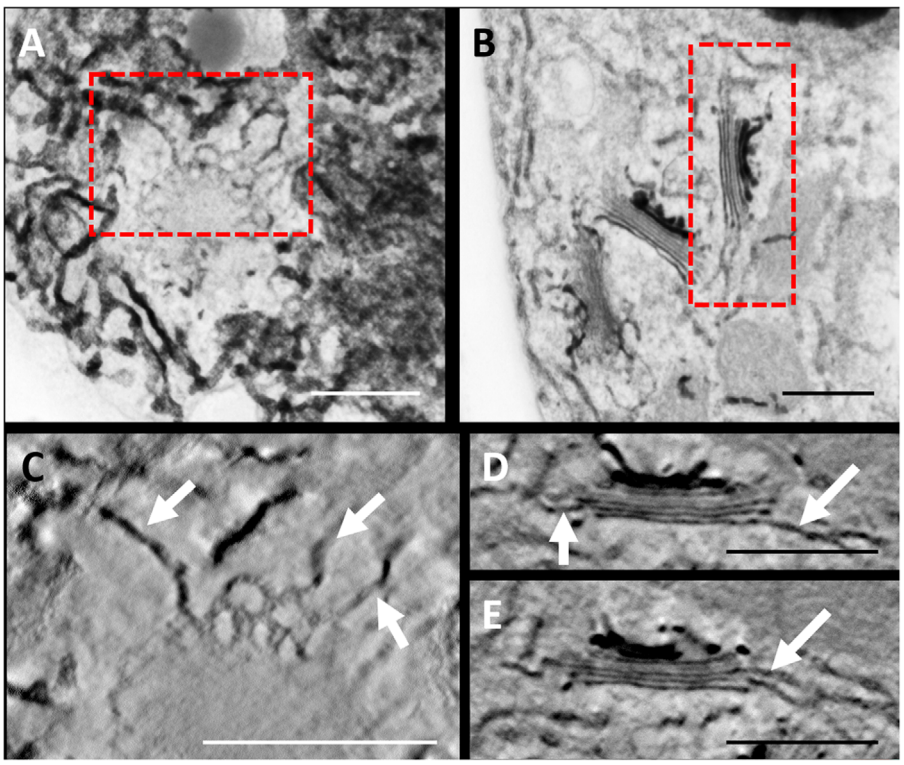

Fig. 3. 3D reconstruction by tomography of the endomembrane system of a ZIO-stained Venus flytrap leaf gland. (A)–(B) TEM micrographs from 10-nm thick optical slices. (C), (D) and (E) are the corresponding electron tomograms. (D) and (E) are made up of different Z depths from the same tomogram. Boxes in (A) and (B) indicate the location of the tomogram data. Arrows indicate prominent connections between the Golgi stacks and ER. Scale bars: 500 nm.

differential ZIO impregnation from the *cis*-most cisternae to the *trans*-most cisternae, highlighting the polarity of the Golgi stack (Fig. 3B). The reticulate nature of the *cis* Golgi (poorly stained here) is enmeshed in a heavily stained ER membrane network (Fig. 3A). This planar view of *cis*-Golgi cisterna suggests multiple connections with the ER. The corresponding tomograms of the two Golgi stacks differentially orientated in space confirm tubular connections between the fenestrated margins of the *cis*-Golgi cisternae and the ER (Figs. 3C,D), as well as between the median cisternae and the ER (Fig. 3E).

3D reconstruction by SBF-SEM provided an even larger volume rendering (Fig. 4). SBF-SEM data captured from within a ZIO-impregnated sample mirror the TEM micrographs presented in Figure 3. The maximum intensity projections of the image stack recorded by SBF-SEM describe Golgi stacks as being tightly enmeshed with the ER network, with ER/cisternal connections at different cisternal levels. ER appears mostly tubular, but some small sheets can be seen. Few if any vesicles are associated with the periphery of these cisternae.

Are these tubular connections the consequence of the sample preparation protocol (chemical fixation/ZIO *en bloc* staining), or are they representative of a functional state of the secretory system? At that stage, the question remains fully open. Analysing the ultrastructure of the endomembrane system through the three main stages of the digestive cycle by high-pressure freezing may contribute to this long-standing question.

Reorganisation of the endomembrane system throughout the digestive cycle: a 2D study using samples fixed by high-pressure freezing

Contrastingly with ZIO impregnated samples, observations on samples prepared with high-pressure freezing fixation protocols (see flow box B in Fig. 1) did not permit to find tubular connections between ER and Golgi. On the other hand, three distinct phases in the secretory activity of the epidermal cells were identified over 6 days (D) of observation: D0 to D1, D1 to D2, D3 to D4 and finally returning to a situation close to the resting stage (not shown) in D5. Tracking of the architectural changes during these three phases is described below.

Ultrastructural organisation in the resting stage (day 0). The main characteristic of secretory cells observed in the resting stage was the occurrence of a large vacuole accompanied by several smaller vacuoles. All vacuoles appeared electron-transparent, presenting rather dispersed and moderately stained structures (Figs. 5A, B). Meanwhile, the early

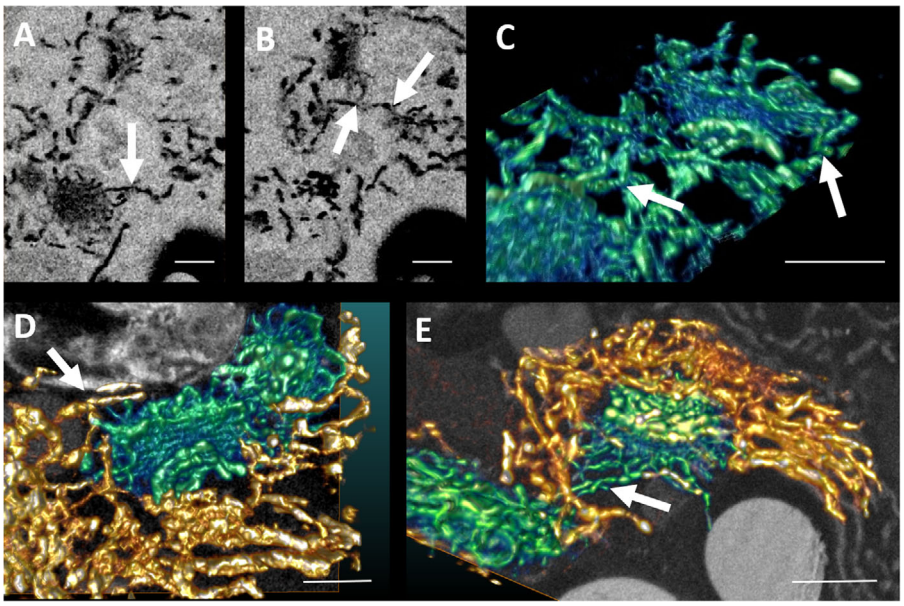

Fig. 4. SBF-SEM. (A)–(B) Images taken of a Venus' flytrap leaf gland cell at different depths within the sample. (C)–(E) Maximum intensity projections of Golgi bodies (blue to green with green indicating the highest electron signal) and ER (orange to yellow, the lighter shades indicating the highest electron signal) showing connections (arrows) between the two. (D) and (E) also show orthoslices through the data in the background of the image. (C) is a reconstruction of the data shown in (A). Scale bars: 500 nm.

compartments of the secretory pathway, that is ER and GA, exhibited a typical plant ultrastructural organisation, with small Golgi stacks made of four to six flattened cisternae dispersed throughout the cytoplasm (Figs. 5C and S1). These were surrounded by small, rare vesicles, suggesting a low secretory activity by exocytosis. This Golgi stack architecture was quite homogeneous throughout the whole GA (Fig. S1). The ER appeared dispersed throughout the cytoplasm displaying tubular profiles. Most ER profiles were heavily decorated with ER-bound ribosomes, suggesting they might actually originate from ER sheets rather than tubules (Fig. 5B). Multivesicular bodies (MVBs) (Fig. 5C) were often observed, enclosing a large number of intraluminal vesicles. The plasma membrane was closely apposed to the cell wall (Fig. 5A). Wall ingrowths, a characteristic of secretory cells (Vaughn *et al.*, 2007), were also observed (Figs. 5B–C, arrows). Atypical membranous features not previously reported in chemically fixed samples were also seen, with complex circular labyrinths (0.5–2 μm size) mixing cytoplasmic and vacuolar networks observed in the vacuolar space (Fig. 5D). These labyrinthic networks will persist and even become more prominent during the digestive cycle (Fig. 6B).

Ultrastructural organisation after stimulation of secretion (day 1 and day 2). Activation of the trap induced profound modifications of the endomembrane system during the first 24–48 h (Fig. 6). One striking aspect of reorganisation concerned the main electron-transparent vacuolar system: the vacuoles became more convoluted, and were apparently breaking down into smaller vacuolar compartments (Fig.6A). The unusual labyrinthic networks were still observed in the vacuolar space of the main vacuolar structure (Fig. 6B). Besides this vacuole population, a heterogenous population of electron-dense vacuoles/vesicles was also observed at this stage. One of these subpopulations was clearly derived from Golgi stacks. A few Golgi stacks still presented the typical profile made of five cisternae described at the resting stage, but most of the Golgi stacks now presented a quite extraordinary profile: they were made of only one to three cisternae, bulging at their extremities and producing large (150–300 nm) electron-dense vesicles (Figs. 6C–E, arrows). The faith of the lost cisternae may be mirrored either by the high vesiculation process which is observed, although dispersal of stray cisternae may occur (Figs. 6F–H), as suggested by the width of some membranous tubular profiles. These images strongly suggest that the Golgi stacks are engaged in the massive secretion of products *en route* to the cell surface. Variations in the electron-dense content of these vesicles may have varied from one Golgi to the next (see supplementary data Fig. S2). On the other hand, aside from this electron-dense Golgi-derived material, another subpopulation of large vesicles (300–500 nm) had their surface marked by a thin electron-dense membrane, enclosing homogenously stained contents (Figs. 6C–E, arrowheads). Do these vesicles derive from Golgi stacks or are they derived from other structures that could not be well-established in these 2D micrographs? One hypothesis is that they may correspond to *trans*-Golgi network (TGN) elements described in Gergely *et al.* (2018). Tubular profiles that associate with those

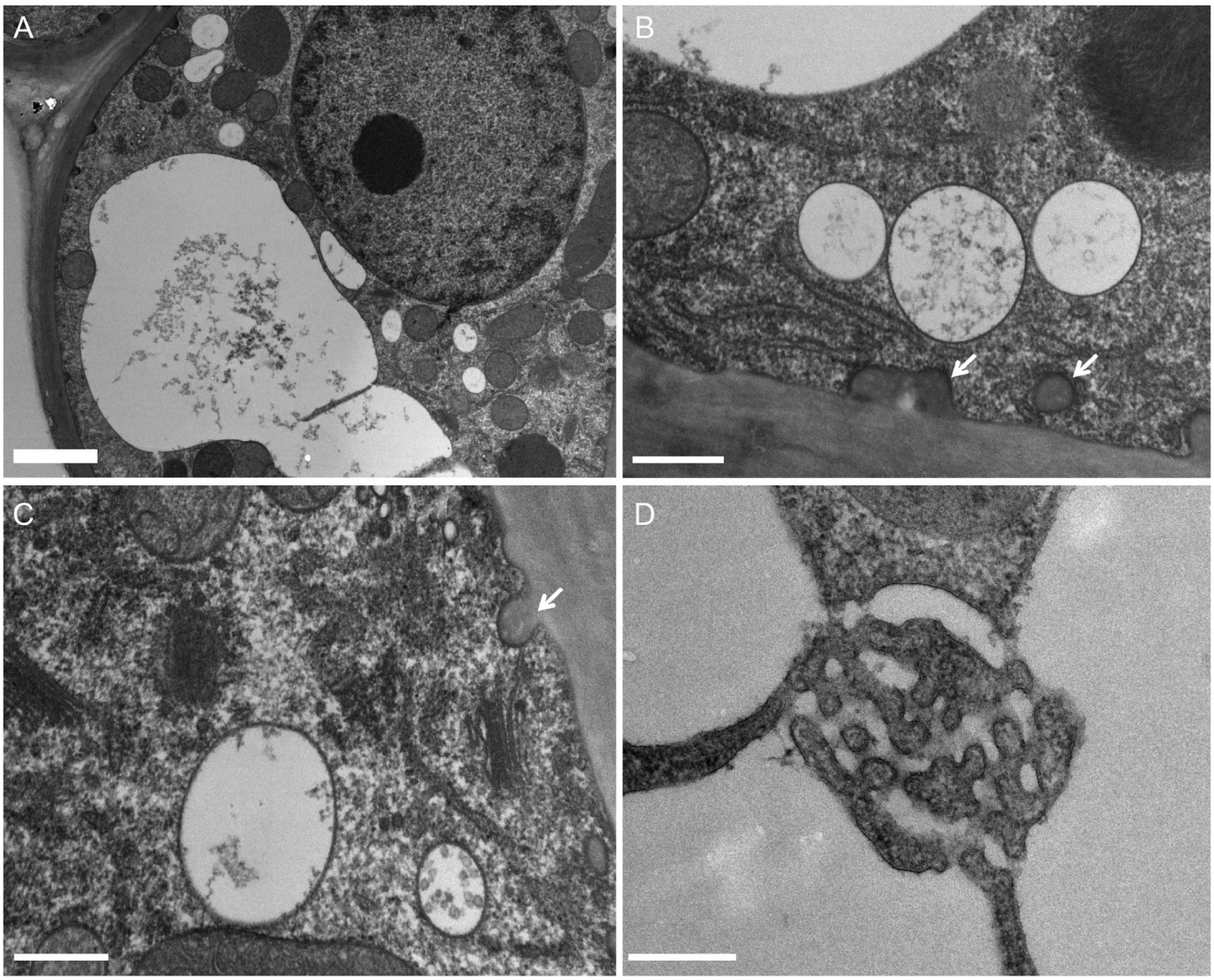

Fig. 5. Ultrastructural organisation of secretory cells of digestive glands in the resting stage (D0). (A) Note the large vacuole together with the occurrence of a few small vacuoles; arrows indicate wall ingrowths. (B) ER, small vacuoles and typical wall ingrowths (arrows). (C) Two Golgi stacks, surrounded by a few small vesicles, made of four to six flat cisternae. Note the multivesicular body (MVB) with intraluminal vesicles and wall ingrowth (arrow), characteristic of secretory cells. (D) Labyrinthic network within the vacuolar space. Scale bar (A): 5 µm; scale bars (B–C–D): 500 nm.

vesicular structures profiles were also observed (Figs. 6F–I). Those could correspond to ER profiles, or, as previously evoked, to stray Golgi cisternae, as the width of the profiles matched the width of the Golgi cisternae (Figs. 6F, H). At this stage, tubular ER was still present throughout the cytoplasm. Micrographs showed small 50–70 nm dense structures in the vicinity of the ER, Golgi stacks, and large vesicles, evoking coated vesicles involved in traffic between compartments (Figs. 6C, E, F, H, I). MVBs were also abundant, with a high number of intraluminal vesicles. The cell surface was still made of the cell wall flanked by a closely apposed plasma membrane (Fig. 6A).

Ultrastructural organisation after stimulation of secretion (day 3). Three days after feeding plants, we observed new ultrastructural features that characterised the secretory cell: an apparent breaking of the vacuolar system, a modification of Golgi secretory activity, and the occurrence of an enlarged periplasmic space filled with osmium-sensitive material, as reported below.

The apparent process of vacuolar remodelling was reinforced, since the vacuolar system was made up of a dense population of small vacuoles (Figs. 7A, B). Some observations even suggested connections between small vacuoles, or fusion events (Fig. 7B). The extent of this connectivity was

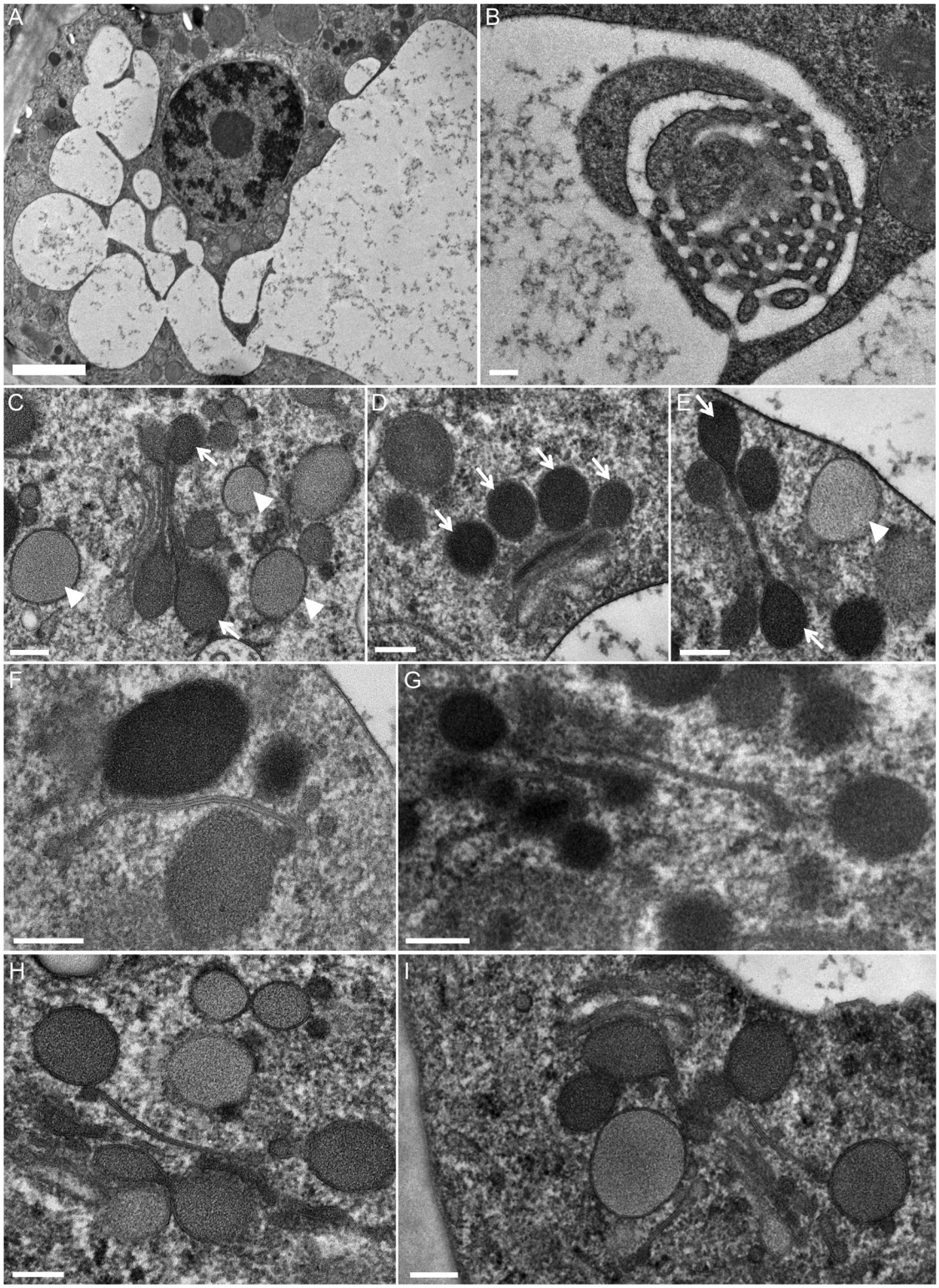

Fig. 6. TEM micrographs of secretory cell ultrastructure 1–2 days after stimulation. (A) Main convoluted vacuole giving rise to interconnected or isolated subcompartments. (B) Labyrinthic network in the vacuolar space. (C)–(E) Drastically altered Golgi stacks. The Golgi stacks, which contain less cisternae, are connected to large secretory vesicles and are full of fine electron-dense material. Note that the luminal electron-density of the vesicles around the Golgi stack is heterogeneous. (F)–(I) ER and tubular structures associated with dense vesicles. Scale bar (A): 2 μm; scale bars (B–I): 200 nm.

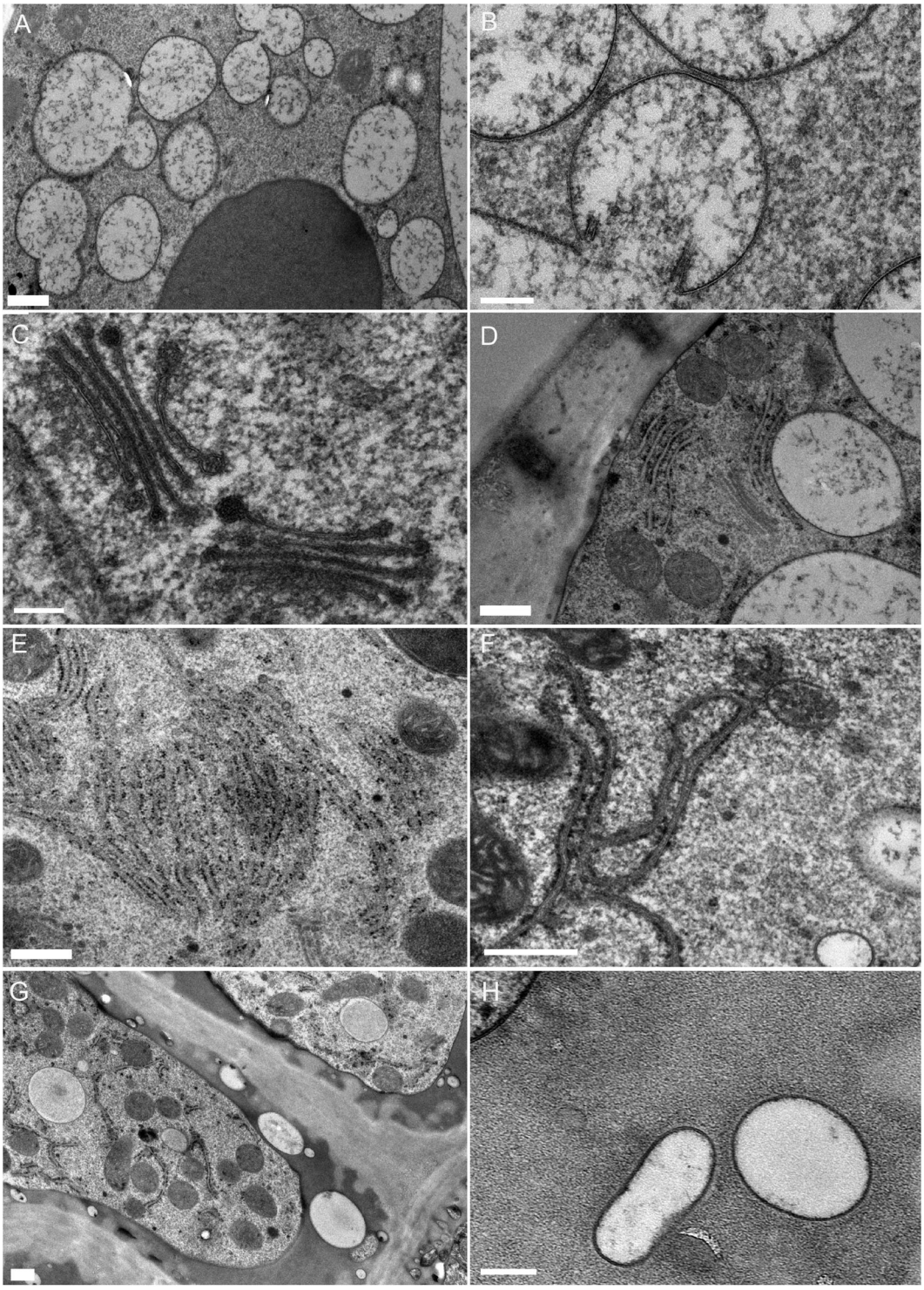

Fig. 7. Ultrastructure of the secretory cells of the digestive glands 3 days after stimulation. (A)–(B) Clusters of small independent or interconnected vacuoles in the cytoplasm. (C) Golgi stacks containing 4–5 cisternae, with small dark vesicles. (D)–(F) ER remodelling: (D) The ER may be closely apposed to the vacuoles; (E) abundant ER organised in stacks; (F) ER branched configurations. (G) Occurrence of a new compartment between the plasma membrane and cell wall (periplasmic space). (H) Detail of the new periplasmic space, with embedded membranous 'pockets'. Scale bars (A–D–E–G): 500 nm; scale bars (B–C–F–H): 200 nm.

investigated by 3D analysis. Labyrinthic networks were rarely observed at this stage. On the other hand, the GA seemed to enter a new cycle of secretion as Golgi stacks were built up again, composed of three to six cisternae (Fig. 7C). At this stage, the massive electron-dense vesicles described earlier were no longer detectable, and were replaced by numerous small electron-dense vesicles budding from the margins of cisternae (Figs. 7C, S3). Golgi stacks appeared extremely or partially curled (Fig. S3). These images still suggest secretory activity, but at a different rate or with a different quality than described before. Contrastingly with the previous stage, structural modifications of the ER network were now often detected, suggesting a complex 3D reorganisation and changes in communication within the cells. For example, the ER could be closely apposed to the vacuolar membranes (Fig. 7D), and clear ER sheets were organised in membranous stacks (Fig. 7E), or present in branched configurations (Fig. 7F). MVBs were rarely observed.

One striking characteristic of secretory cells at this stage is the occurrence of a new space at the cell surface, settling between the plasma membrane and the preexisting cell wall (Figs. 7G–H). We also observed that the plasma membrane had retracted within the cells, compressing the cytosol. This new space was homogenously stained, exhibiting a fine granular content. The texture and density of this new compartment was similar to the contents of the Golgi-derived vesicles observed at D1–D2. Membranous 'pockets' of unknown origin or functions were also observed in this newly created space (Fig. 7H).

These observations suggested the occurrence of a second phase of secretory activity, distinct from the one observed in D1–D2.

Ultrastructural organisation after stimulation of secretion (day 5). After 5 days, the new periplasmic space described in D3 had disappeared and the cell organisation resembled that described in the resting state. Golgi stacks and ER exhibited structural profiles similar to the ones described at D0, and no secretory vesicles were detected around the Golgi stacks. Finally, the main vacuole reformed.

Visualisation of the intra- and interconnections of the vacuolar system, vesicles and ER by array tomography

We found the evolution of the vacuolar system described above (i.e. the apparent fragmentation throughout the digestive cycle) very intriguing. Moreover, the existence of heterogeneous populations of vesicular structures brought into question the origin of these vesicles. In order to further analyse the vacuolar remodelling and occurrence of small vacuolar/vesicular structures, 3D reconstructions of the vacuolar system were made by array tomography.

3D reconstruction of the vacuolar system confirmed that, prior to activation of secretion by prey trapping, the vacuolar system was primarily composed of a main large vacuole with small convolutions (Fig. 8A). 3D reconstruction of such figures showed that the few small vacuoles present in the cytoplasm were actually connected to the main vacuole (Fig. 8A, arrow).

After activation of the trap and triggering of the secretion processes, 2D data clearly revealed a remodelling of the vacuolar system. The 3D volume reconstruction showed that those smaller vacuoles observed in the 2D representation were still clearly associated with a highly complex main vacuolar structure, forming interconnected subvacuolar domains (Figs. 8B, C). Serial sections observed by SEM also permitted focusing on the structural connections between two subvacuolar compartments. The continuum is composed of a tight channel between the two subvacuolar compartments (Fig. 8C). These data suggest the occurrence of constriction or tubularisation events, in contradiction with the term 'fragmentation process' previously evoked from 2D data. Interestingly, the 3D reconstruction of labyrinthic networks observed in the 2D micrographs were positioned at the junction between those subvacuolar compartments (Fig. 8B, arrow), suggesting a peculiar mechanical or physiological role for these areas in the remodelling of the vacuole.

Besides the main vacuolar system that is recognisable by its electron-translucent content, distinct populations of large vesicular structures were also observed in SEM micrographs (Figs. 8E–F). Their content is reminiscent of the cytoplasm. Their 3D reconstruction outlined a complete separation from the vacuolar compartments (Fig. 8D, arrow). When observed in close proximity to the cell surface, they appeared to be surrounded by the plasma membrane (Figs. 8E, D, asterisk). These profiles suggest the occurrence of autophagosomal-like structures, originating from the plasma membrane. They may be related to 'inflows' of membranes to compensate for the massive export of membrane material during the secretory activity observed in the previous stage, and could therefore explain the cytoplasm-like content of these vesicles.

One of the structural characteristics evoked by TEM micrographs at this stage was the remodelling of the ER network. Clear ER sheets were observed (Figs. 8G–I). Array tomography was used to determine whether there was any relationship between the ER and vacuoles (Figs. 8G, H). As shown in Figures 8(H) and (I), the vacuoles seemed to be wrapped on one side by extended ER sheets, suggesting a functional role for ER/vacuole exchanges.

Quantification of vacuolar volume variation between the resting and activated stages of the digestive cycle: LM image analysis

Next, we addressed whether the morphological changes observed in the vacuolar system were related or not to surface/volume changes. As previously shown, stacks of serial sections provided an overview of the volumetric changes in vacuoles within an entire cell. The possibility to perform

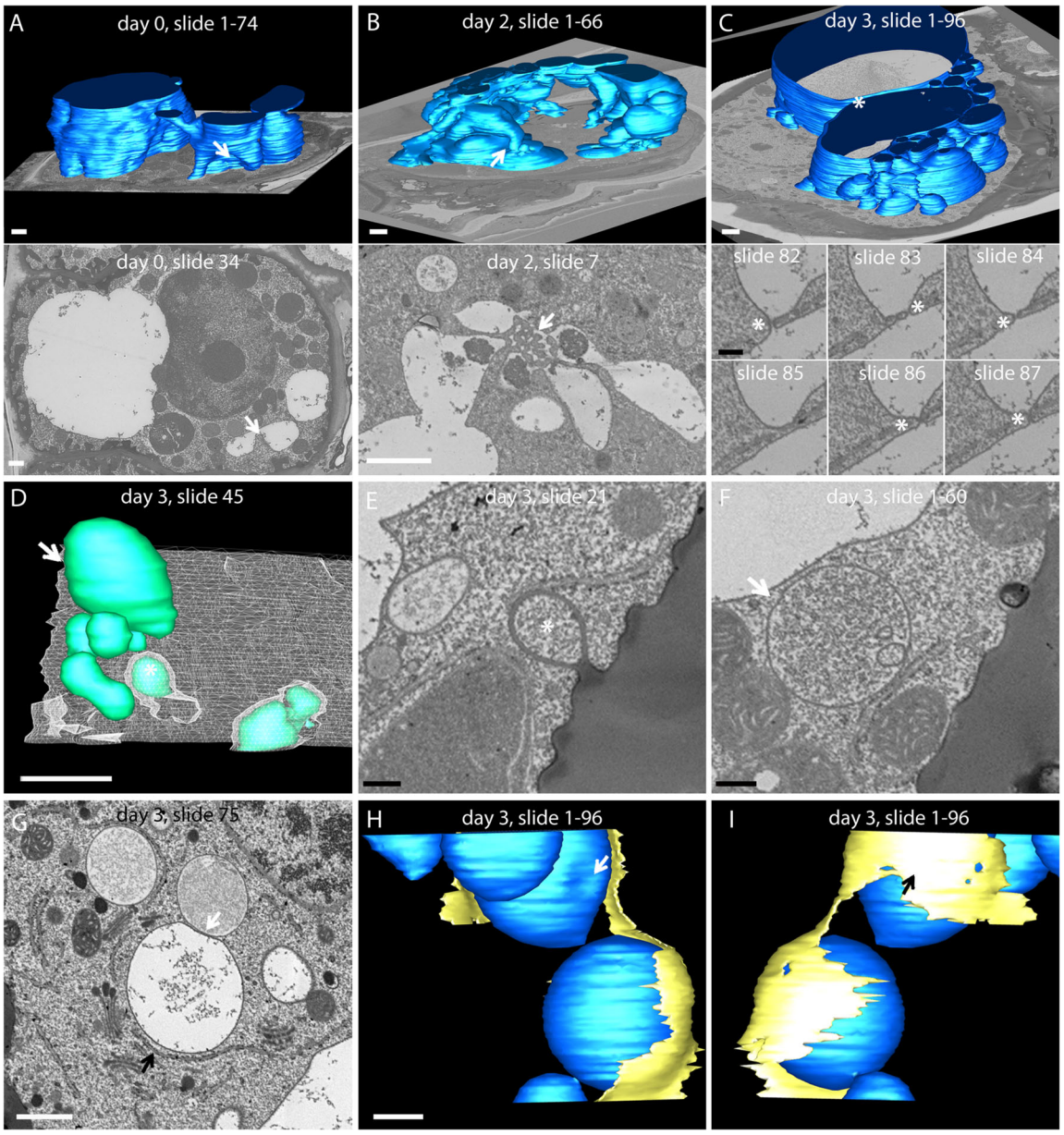

Fig. 8. 3D rendering from array tomography data. (A)–(C) Comparison of the main vacuole 3D structure at the three time points of secretion. (A) Vacuole reconstruction in a resting cell (day 0). Top: modelling of 74 sections (thickness = 50 nm section^{-1}). Bottom: micrograph of slide n°34. White arrows indicate the corresponding position of the micrograph on the modelling. (B) Vacuole reconstruction in a secretory cell 2 days after activation. Top: modelling of 66 sections (thickness = 60 nm section^{-1}). Bottom: detail of micrograph n°7. Labyrinthic network of vacuolar material observed in 2D micrographs (arrow) is positioned between several vacuolar subcompartments. (C) Vacuole reconstruction in a secretory cell 3 days after activation. Top: modelling of 96 sections (thickness = 50 nm section^{-1}). Bottom: detail of serial sections (n°82 to 87) extracted from the image stack modelllised in the upper part. Tubular connections are observed between 2 vacuolar subcompartments (*). (D)–(F) Vesicular structures were localised near the plasma membrane, or even enmeshed in it (day 3). (D) Modelling of 60 sections (thickness = 50 nm) at day 3. White: plasma membrane; green: vesicular structures. Arrow: vesicle observed on the micrograph presented in (F). (*): 3D reconstruction of the structure observed in (E). (E) Micrograph of section n°45 extracted from the model presented in (D). *The corresponding vesicles in the model (D). (F) Micrograph of section n°21 extracted from the model presented in (D). Arrow shows the corresponding vesicles in the model (D). (G)–(I) ER-vacuole contact in activated secretory cells (day 3). (G) Micrograph of section n°75 extracted from the stacks in (H)–(I). White and black arrows show the positions of the corresponding arrows in (H) and (I). (H)–(I) Two views of the reconstruction of the structures observed in G. (H) White arrow corresponds to the white arrow in the micrograph (G). (I) Black arrow corresponds to the black arrow in (G). Blue: vacuole; yellow: ER. White scale bar: 1 μm; black scale bar: 200 nm.

Table 1. Summary of observations made by volume EM approaches.

	D0–D1	D1–D3	D3–D4	D5
Cell wall	Wall ingrowths	Wall ingrowths	Wall ingrowths	Wall ingrowths
Periplasmic space			Enlarged periplasmic space, possibly made of proteins	
Plasma membrane	Closely apposed to the cell wall	Closely apposed to the cell wall ER connections?	Plasma membrane retraction	Closely apposed to the cell wall
Vacuole	Main vacuole, with few subcellular compartments	Convoluted vacuoles, interconnected vacuoles	Interconnected small subvacuoles	Reconstruction of a main vacuole
Polygonal network	Presence of labyrinthic network	Presence of labyrinthic network	Disappearance of a labyrinthic network	Rarely observed
Golgi	4–5 cisternae	Decrease in Golgi cisternae number (2–3 cisternae)	Increase in Golgi cisternae number (4–5 cisternae)	4–5 cisternae
Golgi-associated vesicles	Small and rare	Peak production of massive secretory vesicles (protein content)	Peak production of small secretory vesicles	Resting stage
ER-GA tubular connections	Juniper *et al.* (1982); this study*		Juniper *et al.* (1982); this study*	
Intracytoplasmic vesicles	Rare	Heterogenous populations, at least two types	Small vesicles	Rare
ER	Tubular ER and ER sheets, dispersed throughout the cytoplasm	ER close proximity to the Golgi	Complex ER remodelling and ER/organelle contact sites, suggesting multiple functions	Tubular ER and ER sheets
Multivesicular bodies	Numerous	Numerous	Rarely seen	Numerous

*Note that the number and profiles of cisternae in the Golgi stack suggests that the cells are engaged either in the second phase of the secretory event (D4–D5) or in the early stage (D1–D2).

automatic segmentation based on contrast provided by specific fluorescent labelling was therefore combined with the ability to reconstruct volumes from serial sections.

In order to optimise dye uptake by the sections, D0 and D2 samples were processed without contrasting agents before resin embedding. A combination of DAPI and propidium iodide (PI) was applied in order to differentially stain cell perimeters and vacuoles. Staining of entire ribbons of serial sections affixed to glass coverslips ensured a homogenous contrast throughout the entire preparation (Figs. 9A,B), permitting a clear visualisation of cells and vacuoles (Figs. 9C,D) and facilitating subsequent 3D cell reconstructions (Fig. 9E). Figure 10 illustrates the data extracted from the image analysis of six secretory glands in the resting stage D0 (Fig. 10A) or after two days of trap activation (D2) (Fig. 10B). Cell volumes remained unchanged between the two conditions (data not shown). However, an increase in both vacuolar surface and vacuolar volume in each cell was observed after triggering the secretory process, suggesting that membrane flow to the vacuole may occur.

Discussion

The prey of *Dionaea muscipula* provides an essential source of nutrients such as nitrogen and minerals, as these plants typically grow in soils that are poorly enriched with these components. Trap performance is linked to the ability to quickly digest prey, before reopening for subsequent prey capture. Thus, an efficient trap requires a supporting digestive system, and must be regulated by a specific molecular orchestration within the cells. Here, we used a volume electron microscopy toolbox to learn more about the cellular mechanisms possibly involved in this process.

A combination of 2D and 3D EM approaches provided us with an abundance of data on ultrastructural modifications (Table 1). These approaches are complementary to a previous HVEM study (Juniper *et al.*, 1983), as well as more recent electron tomography observations made at 300 kV by Gergely *et al.* (2018). They are associated with the original feeding strategy of *Dionaea*, and probably outline possible key innovations in secretory processes in the evolution of eukaryotic cells. Importantly, the reported descriptions of secretory events (i.e. timing and intensity) may differ slightly from one experiment to the next, or between laboratories, depending on the very nature of the experimental prey (e.g. liquid versus solid; see also Scala *et al.*, 1969). Intensity or even quality of secretory events may also depend on the physiological state of the trap, performances of which will decrease with the number of cycles (mainly three, but exceptionally four cycles) (Davis *et al.*, 2019). It is also essential to stress that remodelling of the membrane system should probably be considered as a whole that is greater than the sum of its parts.

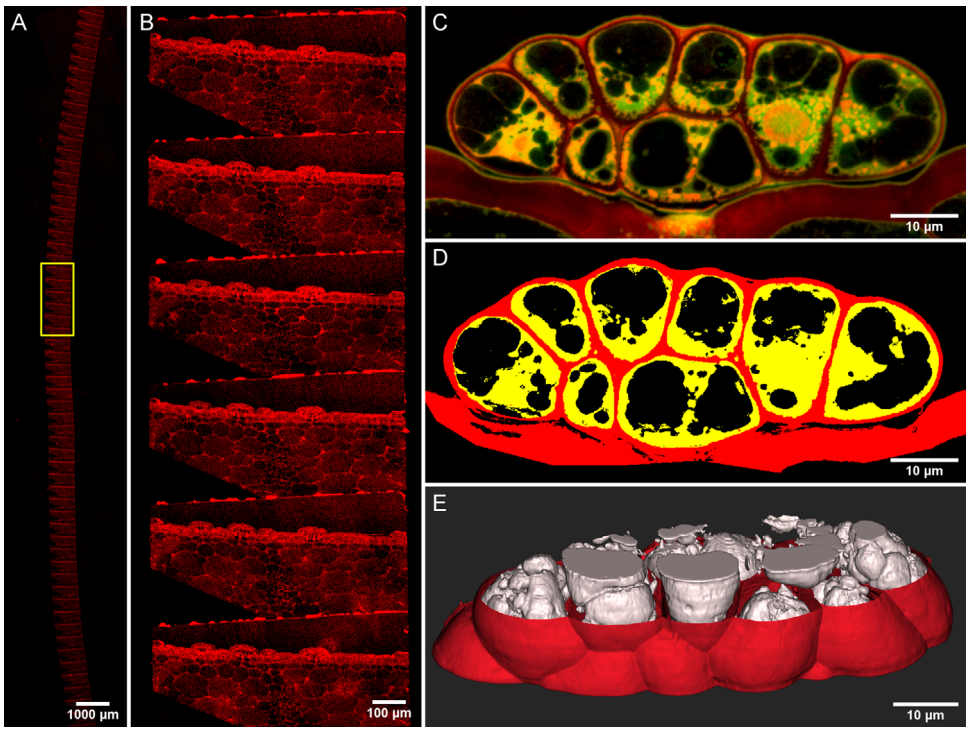

Fig. 9. 3D reconstruction of vacuolar volume from serial sections observed by light microscopy. Successive steps are shown in the volume reconstruction of the secretory gland cells and vacuoles. (A)–(B) Low-magnification fluorescence image of the serial sections stained with DAPI and propidium iodide to generate the automated high-resolution acquisitions. (C) High-resolution dual channel fluorescence image of a single gland section. (D) Result of the segmentation procedure used to generate two masks: cell walls (red) and nonvacuolar cell content (yellow). (E) 3D reconstruction of the cell walls (red) and vacuoles (grey) from the binary masks.

ZIO impregnation and the ER/Golgi relationship: organisational and functional changes in ER–GA exchanges throughout the digestive cycle

One source of debate regarding the reliability of EM data is the variation in observations according to the protocol used in sample preparation. Results showed that membrane continuum was described between ER and Golgi stacks when samples were prepared along a ZIO protocol impregnation process. However, such continuum was never detected when samples were prepared along high-pressure freezing/osmium protocol (this paper; Gergely *et al.*, 2018). Are those ZIO-stained membrane continuum artefactual or do they reveal a physiological trait of the endomembrane system only decipherable by ZIO protocols? Osmium impregnation techniques are the most popular way to increase membrane contrast. These techniques are based on the reduction of osmium tetroxide, which leaves a deposit of osmate or osmium on the surface of membranes or within the cisternal space of membrane-bound organelles. Osmium tetroxide mainly reacts with double bonds that are not present in all lipids. In the ZIO protocol used for this study, osmium reduction was furthermore increased by the addition of zinc iodine osmium mixture, which probably limits the extraction of unbound molecules during dehydration steps.

The ZIO impregnation method could be considered an ideal *en bloc* staining method for the early compartments of the secretory pathway (i.e. the ER, GA, and nuclear membranes), it does not always enhance the tonoplast, it never labels the plasma membrane, and hardly ever stains Golgi-derived or associated vesicles. The duration of staining may affect the whole impregnation process and should be tested for each biological sample (4–12 h for *Dionaea*; C. Hawes, personal communication). Its ability to stain membrane structures may therefore reveal a highly sensitive and complex cytochemical reaction *in cellulo*, linked to specific molecular arrangements within the membranes. It therefore cannot be excluded that the association of chemical fixation and heavy osmiophilic response obtained with ZIO protocol may enhance characteristics not detectable by some other means. The information extracted from ZIO observations should therefore be considered as solid data. In this study, a strong staining gradient is typically observed across the sample (due to uneven fixation speed or intensity and/or uneven penetration of the chemicals during impregnation process) permitting the selection of regions of interest. The ER–Golgi continuum observed in this study has been detected by ZIO impregnation in several biological materials (Harris, 1979; Hawes, 1981; Hawes *et al.*, 1981; Harris & Oparka, 1983; Mérigout *et al.*, 2002; Képès *et al.*, 2004) but not all, suggesting that the occurrence of such

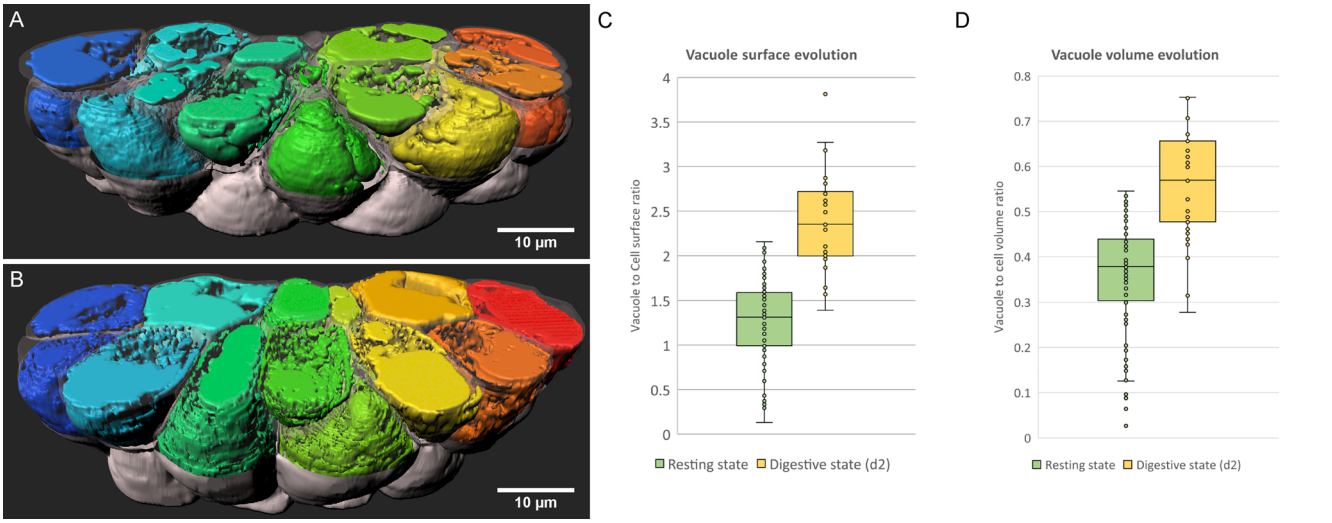

Fig. 10. Quantification of vacuolar morphology change from light microscopy 3D reconstructions. Representative volume rendering of a secretory gland (grey) and its vacuolar system (using rainbow LUT, one colour per cell) in the resting (A) or digestive stage (B). (C) Quantification of the vacuole surface change between resting and digestive stages. The vacuole surface is presented as the surface of all the vacuoles within a cell normalised by the cell surface. (D) Quantification of the vacuole volume change between the resting and digestive stages. The vacuole volume is presented as the volume of all the vacuoles within a cell normalised by the cell volume. Resting stage samples: 70 cells. Digestive stage samples: 34 cells.

connections may be dependent on the type of secretory activity of the cell. For example, in carbohydrate-secreting cells that specialise in polysaccharide secretion, connections between the Golgi and ER are rarely observed (as in maize root caps, bean leaf palisade tissue, and elongating bean roots). Meanwhile, in protein-secreting cells, connections between the tubular ER and Golgi are observed across the cisternal stack (Juniper *et al.*, 1982).

Taking into account these considerations, we believe that the tubular ER–GA connections observed by electron tomography and SBF-SEM at the D4–D5 or D0–D1 stages are truly representative of a specific functional organisation in *Dionaea muscipula*. Such a tubular continuum, detectable mainly (if not only) by ZIO approach, may correspond to an efficient transfer mechanism for lipids and/or proteins between the ER and GA, especially for use in rapidly resetting the molecular GA machinery.

The HPF/freeze-substitution protocol: two distinct phases of protein secretion occur throughout the digestive cycle

The osmium *en bloc* staining associated with the HPF protocol provided 'shades of grey' among the stained structures. This procedure stains membranes enriched in unsaturated lipids, interacts with proteins (producing electron-dense material in secretory vesicles), and reveals a fair amount of the ultrastructural content, especially the occurrence of heterogeneous vesicles/vacuole-like compartments. However, it does not selectively stain polysaccharide-containing vesicles or cell walls. It therefore constitutes an appropriate staining protocol to track the trafficking of a massive production of cargo proteins.

Based on our observations, two phases of protein secretion could be observed. In the first, there is a massive peak involving high activity in both the ER and GA. Golgi stacks exhaust themselves by producing massive protein-stained vesicles. Meanwhile, the ER exhibits tubular connections or close contacts with a subpopulation of vesicles, which suggests the occurrence of ER-derived secretory vesicles that may bypass the Golgi stacks. Such by-passes have been described for instance in case of ER-to-vacuole transports (Pereira *et al.*, 2013). Direct contact between the ER and plasma membrane has also been suggested to be involved in protein release to the cell surface in previous studies (Juniper *et al.*, 1982). ER to cell surface secretion has been described in the extrafloral nectary of *Abutilon* where the prenectar is loaded into a specialised form of ER. The second phase of endomembrane activity was observed as a distinct architecture of the GA and ER network. Golgi stacks being rebuilt still presented dense electron vesicles at the margins of their cisternae (although they were much smaller than in the previous step), and were surrounded by numerous small (coated) vesicles. Interestingly, some of the Golgi stacks were often curled or partially curled. Such Golgi profiles have been previously described (Lütz-Meindl *et al.*, 2016), in a different functional/physiological background probably related to stress. It may be related either to a differential membrane growth (*cis* sides growing faster than *trans* sides), or to the settings of the molecular machinery for cisternae stacking. At this stage, the ER may be involved in sustaining the homeostasis of lipids and proteins in different subcellular compartments, as suggested by the high reorganisation

of its network (i.e. branched configurations in close contact with vacuoles and Golgi stacks). These results suggesting two secretory phases are in agreement with the biphasic secretion curve described by the fluorescent casein assay and are possibly related to the different nature of secreted proteins (Gergely *et al.*, 2018).

Taking these considerations into account, we believe that the first secretion peak is part of a rapid response to deliver digestive fluids to the cell surface, which delivers the needed stock of digestive materials 'on site'. The second peak of activity could then be associated with the reconstruction of the Golgi, ER and vacuolar machinery, in order to prepare for a subsequent round of prey capture. As stated by Gergely *et al.* (2018), *'cells of secretory glands are "overbuilt" to permit the stimulated cells to quickly provide the needs in digestive enzymes'*.

The Dionaea *feeding strategy involves a novel Golgi morphodynamic process*

The morphodynamics of the Golgi apparatus in *Dionaea muscipula* may add to our general understanding of plant Golgi biology. As in other plant secretory cells, a massive transport to the cell surface of secretory products from the bulging margin of the Golgi cisternae was observed in order to accommodate the cell's needs. However, these ultrastructural profiles were previously observed in the massive production of polysaccharides (instead of proteins) *en route* to the cell surface by a default pathway, leading to the description of plant Golgi as a 'polysaccharide factory' (Driouich *et al.*, 1993). In contrast, the *Dionaea muscipula* GA acts as a true 'protein factory'. Moreover, in plants, the ability to produce proteins is often associated with the production of storage proteins at the most *trans* cisternae of the GA, which are targeted to the vacuolar compartment by specific receptors. Similarly, in mammalian cells specialised in protein secretion, proteins are packaged in secretory vesicles at the *trans* side of the Golgi before their storage in secretory granules (Rambourg *et al.*, 1992). However, in *Dionaea muscipula*, most of the cisternae are involved in secreting the dense vesicles, which are probably directed by bulk flow (*via* a default pathway) to the cell surface for immediate use. *Dionaea* therefore appear to employ a novel mechanism that uses the pleiomorphy/plasticity of the GA in order to optimise the rapid delivery of newly synthesised proteins, branding the plant Golgi stack as an adjustable protein factory.

Our *Dionaea* data also suggest that the capacity to produce massive secretory products may be driven rather by mechanical forces than by a specific molecular machinery. The 'bulging' event occurring at the margins of cisternae may be the result of the accumulation of a product, indistinctly from its nature. Protein processing (such as glycosylation) may occur in the central plain core of the Golgi, and processed proteins could therefore be pushed towards the fenestrated margins of the Golgi cisternae by an unknown mechanisms, until mechanical fission of the membranes and vesicle release from the cisternal structure.

Taken together, these data highlight a certain pleiomorphy in the cisternae stacking, which shakes up the well-established 'cis/median/trans' hierarchical organisation model, and reinforces the hypothesis of a (highly adaptative) cisternal maturation process in plant Golgi biology.

Volume EM approaches and the release of digestive enzymes: when mechanics rejoin physiology

During the first peak of secretion (D2–D3), a new cell surface area emanating from Golgi-derived secretory vesicles is built and the plasma membrane is pushed away from the cell surface. At the same time, *Dioneae muscipula* secretory cells enclose a vacuolar component that is remodelled into multiple and connected subcompartments. The connections between these subvacuolar compartments are extremely complex due to an unusual labyrinth of unknown function (which may function as a mechanical node to resist volume changes) and the presence of thin channels. All of these events have to be part of the same arrangement: delivering digestive enzymes as quickly as possible to increase trap efficiency.

The punctual and temporary enlargement of the periplasmic space probably constitutes a reservoir made of freshly synthesised enzymes for immediate use. The Golgi machinery plays a crucial role in the filling of this periplasmic space, corresponding to the first peak in secretory activity observed on day 2. But what about the emptying process?

Since this is the first time to our knowledge that a vacuolar continuum has been shown in *Dionaea muscipula*, it is tempting to propose a functional role for vacuolar remodelling in accommodating the set-up of a new reservoir, as well as in its emptying. The vacuolar compartment has indeed been frequently compared to an osmometer that regulates both the cell volume conditioning axis of cell growth, and cell homeostasis (Reisen *et al.*, 2005). The progressive and reversible remodelling of the main vacuole in a complex and convoluted network may help in the continuous adjustment of osmotic pressure for secretory events. Earlier studies have suggested a mechanical interplay between the distribution of forces within cells, provoking the exit of fluid from the vacuole and the cell towards the cell surface and contributing to the extrusion of the 'digestive fluid' (Heslop-Harrison & Knox, 1971; Heslop-Harrison, 1975). When returning to a main central vacuole, the vacuole may grow again in size through the addition of new membranes delivered by the recycling machinery either through multivesicular bodies, endosomes or autophagosome-like compartments (see also Cui *et al.*, 2019 for discussion on vacuole constriction).

The function of vacuoles as acidic and catabolic compartments is also important in maintaining cell homeostasis in *Dionaea*. These lytic vacuoles may favour the recycling of nutrients obtained from prey digestion, by processing nutrients

in amino acids and releasing them in the cytoplasm, but they are also essential when cells are not properly fed. However, pathways for the internalisation of nutrients and their further use by *Dionaea* cells have been poorly documented. Such traffic may explain the presence of heterogeneous vesicles in the cytoplasm at D2–D3 during the high peak of secretion, where outflows may meet with inflows. In addition, the recycling of membranes by endocytic mechanisms needs to occur in order to counterbalance the secretory process. The involvement of specific internalisation mechanisms may also take place in the final distribution of digested prey nutrients. The fact that the vacuolar volume increases throughout the digestive process (despite its remodelling) suggests that some of these inflow events actually end up in the main vacuole, either for further processing of nutrients or as a means to replenish the vacuole's stock of permanent lytic enzymes.

Conclusions and perspectives

The delivered secretory product that we studied here is a unique biological fluid, comparable in many ways to the saliva of heterotrophic organisms (Humphrey & Williamson, 2001). The subcellular features of the secretory cells of *Dionaea muscipula* outline key innovations in the organisation of plant cell compartmentalisation that are used to cope with specific cell needs, such as the full use of the Golgi apparatus as a protein factory, and the ability to create protein reservoirs in the periplasmic space. Shape-derived forces of the pleiomorphic vacuole may act as signals to accompany the sorting and entering flows of the cell. The challenge is now to place in their context the molecular regulators of this digestive response that have been suggested by sequencing programs. This should include the COP (Gergely *et al.*, 2018) transport machinery in addition to well-known molecular, Rab and SNARES cascades involved in membrane trafficking, as well as players involved in modification of the cytoskeleton and mechanotransduction. Several biotechnology groups around the world are now engaged in sequencing carnivorous plants in order to identify the signalling pathways that are triggered by prey capture. Altogether, this work reveals a probable combination of mechanical and structural complexity underlying secretory cell organisation, and puts forward the question of trap efficiency in plant biology.

Acknowledgements

We thank Michaël Trichet (IBPS electron microscopy core facility) for his expertise in SEM and array tomography. We thank Jake Richardson for collecting part of the data shown in Figure 3. This work benefited from the expertise of the light microscopy facilities at the Imagerie-Gif (http://www.i2bc.paris-saclay.fr/spip.php?article278). This core facility is a member of the Infrastructures en Biologie Santé et Agronomie (IBiSA), and is supported by the French National Research Agency under the Investments for the Future programs 'France-BioImaging', (ANR-10-INBS-04-01), the 'Saclay Plant Science' Labex (ANR-11-IDEX-0003-02), and the Equipex Morphoscope (ANR-11-EQPX-0029).

References

Bal, A.K. & Payne, J.F. (1972) Endoplasmic reticulum activity and cell wall breakdown in quiescent root meristems of *Allium cepa* L. *Z. Für Pflanzenphysiol.* **66**, 265–272.

Berg, S., Kutra, D., Kroeger, T. *et al.* (2019) Ilastik: interactive machine learning for (bio)image analysis. *Nat. Methods* **16**, 1226–1232.

Borrett, S. & Hughes, L. (2016) Reporting methods for processing and analysis of data from serial block face scanning electron microscopy. *J. Microsc.* **263**, 3–9.

Cui, Y., Cao, W., He, Y. *et al.* (2019) A whole-cell electron tomography model of vacuole biogenesis in Arabidopsis root cells. *Nat. Plants* **5**, 95–105.

Darwin, C. R. (1875). *Insectivorous Plants*. London: John Murray.

Davis, A.L., Babb, M.H., Lowe, M.C., Yeh, A.T., Lee, B.T. & Martin, C.H. (2019) Testing Darwin's hypothesis about the wonderful venus flytrap: marginal spikes form a "horrid prison" for moderate-sized insect prey. *Am. Nat.* **193**, 309–317.

Driouich, A., Faye, L. & Staehelin, A. (1993) The plant Golgi apparatus: a factory for complex polysaccharides and glycoproteins. *Trends Biochem. Sci.* **18**, 210–214.

Fukushima, K., Fang, X., Alvarez-Ponce, D. *et al.* (2017) Genome of the pitcher plant Cephalotus reveals genetic changes associated with carnivory. *Nat. Ecol. Evol.* **1**, 0059.

Gergely, Z.R., Martinez, D.E., Donohoe, B.S., Mogelsvang, S., Herder, R., & Staehelin, L.A. (2018) 3D electron tomographic and biochemical analysis of ER, Golgi and trans Golgi network membrane systems in stimulated Venus flytrap (*Dionaea muscipula*) glandular cells. *J Biol Res (Thessalon)* **25**, 15.

Harris, N. (1979) Endoplasmic reticulum in developing seeds of *Vicia faba*. A high voltage electron microscope study. *Planta* **146**, 63–69.

Harris, N. & Oparka, K.J. (1983) Connections between dictyosomes, ER and GERL in cotyledons of mung bean (Vigna radiata L.). *Protoplasma* **114**, 93–102.

Hawes, C. & Satiat-Jeunemaitre, B. (2001) *Plant Cell Biology: A Practical Approach*. UK: Oxford University Press.

Hawes, C.R. (1981) Applications of high voltage electron microscopy to botanical ultrastructure. *Micron 1969* **12**, 227–257.

Hawes, C.R., Juniper, B.E. & Horne, J.C. (1981) Low and high voltage electron microscopy of mitosis and cytokinesis in maize roots. *Planta* **152**, 397–407.

Hawes, C.R.1., Juniper, B.E. & Horne, J.C. (1981) Low and high voltage electron microscopy of mitosis and cytokinesis in maize roots. *Planta* **152**(5), 397–407.

Heslop-Harrison, Y. (1975) Enzyme release in carnivorous plants. *Front. Biol.* **43**, 525–578.

Heslop-Harrison, Y. & Knox, R.B. (1971) A cytochemical study of the leaf-gland enzymes of insectivorous plants of the genus Pinguicula. *Planta* **96**, 183–211.

Hughes, L., Hawes, C., Monteith, S. & Vaughan, S. (2014) Serial block face scanning electron microscopy – the future of cell ultrastructure imaging. *Protoplasma* **251**, 395–401.

Humphrey, S.P. & Williamson, R.T. (2001) A review of saliva: normal composition, flow, and function. *J. Prosthet. Dent.* **85**, 162–169.

James Morré, D., Kartenbeck, J. & Franke, W.W. (1979) Membrane flow and interconversions among endomembranes. *Biochim. Biophys. Acta BBA – Rev. Biomembr.* **559**, 71–152.

Juniper, B.E., Hawes, C.R. & Horne, J.C. (1982) The relationships between the dictyosomes and the forms of endoplasmic reticulum in plant cells with different export programs. *Bot. Gaz.* **143**, 135–145.

Juniper, B.E., Robins, R.J. & Joel, D.M. (1989) *The Carnivorous Plants*. Academic Press, London, UK.

Képès, F., Rambourg, A. & Satiat-Jeunemaître, B. (2004) Morphodynamics of the secretory pathway. *International Review of Cytology*, vol. **242**, pp. 55–120. Germany: Elsevier, Inc.

Kiss, J.Z., Giddings, ThH, Staehelin, L.A. & Sack, F.D. (1990) Comparison of the ultrastructure of conventionally fixed and high pressure frozen/freeze substituted root tips of Nicotiana and Arabidopsis. *Protoplasma* **157**, 64–74.

Kittelmann, M., Hawes, C. & Hughes, L. (2016) Serial block face scanning electron microscopy and the reconstruction of plant cell membrane systems. *J. Microsc.* **263**, 200–211.

Kremer, J.R., Mastronarde, D.N. & McIntosh, J.R. (1996) Computer visualization of three-dimensional image data using IMOD. *J. Struct. Biol.* **116**, 71–76.

Lichtner, F.T. & Williams, S.E. (1977) Prey capture and factors controlling trap narrowing in Dionaea (Droseraceae). *Am. J. Bot.* **64**, 881–886.

Luttge, U. (1971) Structure and function of plant glands. *Annu. Rev. Plant Physiol.* **22**, 23–44.

Lütz-Meindl, U., Luckner, M., Andosch, A. & Wanner, G. (2016) Structural stress responses and degradation of dictyosomes in algae analysed by TEM and FIB-SEM tomography: structural stress responses and degradation of dictyosomes in algae. *J. Microsc.* **263**, 129–141.

Marion, J., Le Bars, R., Satiat-Jeunemaitre, B. & Boulogne, C. (2017) Optimizing CLEM protocols for plants cells: GMA embedding and cryosections as alternatives for preservation of GFP fluorescence in Arabidopsis roots. *J. Struct. Biol.* **198**, 196–202.

Mérigout, P., Képès, F., Perret, A.-.M., Satiat-Jeunemaitre, B. & Moreau, P. (2002) Effects of brefeldin A and nordihydroguaiaretic acid on endomembrane dynamics and lipid synthesis in plant cells. *FEBS Lett.* **518**, 88–92.

Pereira, C., Pereira, S., Satiat-Jeunemaitre, B. & Pissarra, J. (2013) Cardosin A contains two vacuolar sorting signals using different vacuolar routes in tobacco epidermal cells. *Plant J.* **76**, 87–100.

Plachno, B.J., Adamec, L., Lichtscheidl, I.K., Peroutka, M., Adlassnig, W. & Vrba, J. (2006) Fluorescence labelling of phosphatase activity in digestive glands of carnivorous plants. *Plant Biol.* **8**, 813–820.

Rambourg, A., Clermont, Y., Chrétien, M. & Olivier, L. (1992) Formation of secretory granules in the Golgi apparatus of prolactin cells in the rat pituitary gland: a stereoscopic study. *Anat. Rec.* **232**, 169–179.

Reisen, D., Marty, F. & Leborgne-Castel, N. (2005) New insights into the tonoplast architecture of plant vacuoles and vacuolar dynamics during osmotic stress. *BMC Plant Biol.* **5**, 13.

Robins, R.J. (1976) The nature of the stimuli causing digestive juice secretion in *Dionaea muscipula* Ellis (Venus's flytrap). *Planta* **128**, 263–265.

Robins, R.J. & Juniper, B.E. (1980a) The secretory cycle of *Dionaea muscipula* Ellis. *New Phytol.* **86**, 279–296.

Robins, R.J. & Juniper, B.E. (1980b) The secretory cycle of *Dionaea muscipula* Ellis. *New Phytol.* **86**, 297–311.

Robins, R.J. & Juniper, B.E. (1980c) The secretory cycle of *Dionaea muscipula* Ellis. *New Phytol.* **86**, 313–327.

Robins, R.J. & Juniper, B.E. (1980d) The Secretory cycle of *Dionaea muscipula* Ellis Iv. The enzymology of the secretion. *New Phytol.* **86**, 401–412.

Samuels, A.L., Giddings Jr, T.H. & Staehelin, L.A. (1995) Cytokinesis in tobacco BY-2 and root tip cells: a new model of cell plate formation in higher plants. *J. Cell Biol.* **130**, 1345–1357.

Scala, J., Iott, K., Schwab, D.W. & Semersky, F.E. (1969) Digestive secretion of *Dionaea muscipula* (Venus's flytrap). *Plant Physiol.* **44**, 367–371.

Scala, J., Schwab, D. & Simmons, E. (1968) The fine structure of the digestive gland of Venus's flytrap. *Am. J. Bot.* **55**, 649–657.

Schneider, C.A., Rasband, W.S. & Eliceiri, K.W. (2012) NIH Image to ImageJ: 25 years of image analysis. *Nat. Methods* **9**, 671–675.

Schwab, D.W., Simmons, E. & Scala, J. (1969) Fine structure changes during function of the digestive gland of Venus's-Flytrap. *Am. J. Bot.* **56**, 88–100.

Seguí-Simarro, J.M., Austin, J.R., White, E.A. & Staehelin, L.A. (2004) Electron tomographic analysis of somatic cell plate formation in meristematic cells of Arabidopsis preserved by high-pressure freezing. *Plant Cell* **16**, 836–856.

Thevenaz, P., Ruttimann, U.E. & Unser, M. (1998) A pyramid approach to subpixel registration based on intensity. *IEEE Trans. Image Process.* **7**, 27–41.

Unzelman, J.M. & Healey, P.L. (1974) Development, structure, and occurrence of secretory trichomes of Pharbitis. *Protoplasma* **80**, 285–303.

Vaughn, K.C., Talbot, M.J., Offler, C.E. & McCurdy, D.W. (2007) Wall ingrowths in epidermal transfer cells of vicia faba cotyledons are modified primary walls marked by localized accumulations of arabinogalactan proteins. *Plant Cell Physiol.* **48**, 159–168.

Volkov, A.G., Carrell, H. & Markin, V.S. (2009) Biologically closed electrical circuits in Venus flytrap. *Plant Physiol.* **149**, 1661–1667.

Supporting Information

Additional supporting information may be found online in the Supporting Information section at the end of the article.

Fig. S1. Golgi stacks in the resting stage (D0) are made of four to seven thin cisternae, surrounded by small vesicles. Scale bars: 200 nm.

Fig. S2. Days 1–2 after stimulation: Golgi stacks are frequently made of two to five cisternae, presenting bulging vesicles at the cisternae margins. Scale bars: 200 nm.

Fig. S3. Ultrastructure of Golgi stacks 3 days after stimulation.